SCIENTIFIC REPORTS

OPEN

Received: 07 April 2015
Accepted: 28 September 2015
Published: 23 October 2015

$Ba(Zn_{1-2x}Mn_xCu_x)_2As_2$: A Bulk Form Diluted Ferromagnetic Semiconductor with Mn and Cu Codoping at Zn Sites

Huiyuan Man[1,2], Shengli Guo[1,2], Yu Sui[3], Yang Guo[4], Bin Chen[4], Hangdong Wang[4], Cui Ding[1,2] & F.L. Ning[1,2]

We report the synthesis and characterization of a bulk form diluted magnetic semiconductor $Ba(Zn_{1-2x}Mn_xCu_x)_2As_2$ ($0.025 \le x \le 0.2$) with the crystal structure identical to that of "122" family iron based superconductors and the antiferromagnet $BaMn_2As_2$. No ferromagnetic order occurs with (Zn, Mn) or (Zn, Cu) substitution in the parent compound $BaZn_2As_2$. Only when Zn is substituted by both Mn and Cu simultaneously, can the system undergo a ferromagnetic transition below $T_C \sim 70$ K, followed by a magnetic glassy transition at $T_f \sim 35$ K. AC susceptibility measurements for $Ba(Zn_{0.75}Mn_{0.125}Cu_{0.125})_2As_2$ reveal that T_f strongly depends on the applied frequency with $v_0/v = \left(T_f/19 - 1\right)^{-8.3}$ and a DC magnetic field dependence of $T_f(H) \propto 1 - bH^{0.55}$, demonstrating that a spin glass transition takes place at T_f. As large as −53% negative magnetoresistance has been observed in $Ba(Zn_{1-2x}Mn_xCu_x)_2As_2$, enabling its possible application in memory devices.

The successful fabrication of III-V diluted magnetic semiconductors (In, Mn)As and (Ga, Mn)As through low temperature molecular beam epitaxy (LT-MBE) has opened up a new window for the study of magnetic semiconductors[1–5]. It is proposed that the Curie temperature would reach room temperature with high enough spin and carrier densities[6]. Nevertheless, the low solid solubility of Mn^{2+} for Ga^{3+} makes it difficult to enhance the concentration of Mn. As of today, the highest Curie temperature, T_C, of (Ga, Mn)As films has been reported as 200 K[7]. On the other hand, Mn^{2+} substituting for Ga^{3+} introduces not only carriers but also local moments, and some Mn^{2+} enter interstitial sites or even As sites, which makes it difficult to separate the charges and spins, and investigate their individual influences on the ferromagnetism. Seeking for new DMS materials that have higher chemical solubility of magnetic atoms and whose carrier density and spin density can be controlled separately may be helpful to improve T_C and understand the mechanism of the ferromagnetic ordering[8].

Recently, many novel DMSs that are derivatives of Fe-based superconductors have been reported[8–19]. It has been shown from NMR[20] and μSR measurements that the ferromagnetism in $(BaK)(ZnMn)_2As_2$[9], Li(Zn, Mn)As[10], (La, Ba)(Zn, Mn)AsO[12] and Li(Zn, Mn)P[21] are homogeneous, i.e., the long range ferromagnetic ordering is arising from the Mn atoms doped at Zn sites, instead of Mn related magnetic impurities. Furthermore, μSR results demonstrated that these bulk form DMSs share the same mechanism for the ferromagnetic ordering as that of (Ga, Mn)As[22]. These bulk form DMSs have the advantages of decoupled spin and carrier doping, and the carrier densities can be controlled and tuned, which overcomes the low carrier densities encountered in II-VI DMS[23]. These systems are isostructural to its

[1]Department of Physics, Zhejiang University, Hangzhou 310027, China. [2]Collaborative Innovation Center of Advanced Microstructures, Nanjing 210093, China. [3]Center for Condensed Matter Science and Technology, Department of Physics, Harbin Institute of Technology, Harbin, 150001, China. [4]Department of Physics, Hangzhou Normal University, Hangzhou 310016, China. Correspondence and requests for materials should be addressed to F.L.N. (email: ningfl@zju.edu.cn)

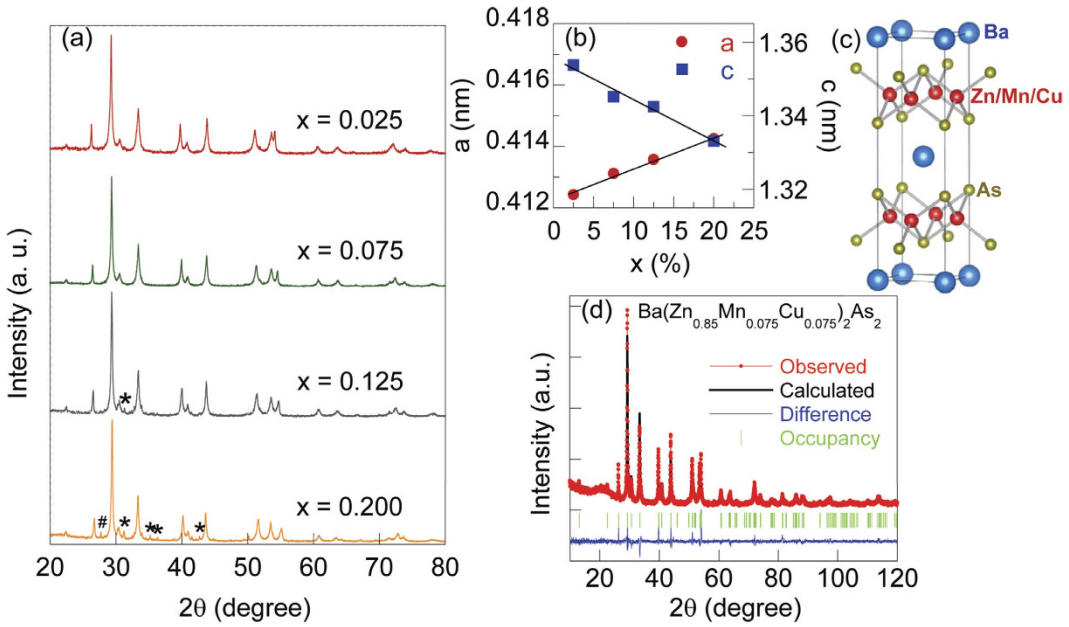

Figure 1. Structural properties of $Ba(Zn_{1-2x}Mn_xCu_x)_2As_2$. (**a**) The X-ray diffraction patterns of $Ba(Zn_{1-2x}Mn_xCu_x)_2As_2$ ($x = 0.025, 0.075, 0.125, 0.20$). Traces of $BaZn_2As_2$ with space group Pnma (*) and impurity Ba_3As_{14} (#) are marked; (**b**) The systematic change of the lattice constants a (red filled circles) and c (blue filled squares) with x. (**c**) The layered crystal structure. (**d**) The Rietveld refinement of the powder X-ray diffraction for the $x = 0.075$ sample.

variants, i.e., antiferromagnets and superconductors with lattice matching within 5%, which provides the the possibility to make junctions with these materials thorough the As layer[19]. In addition, the bulk form specimens would enable the magnetic techniques to provide complementary information at a microscopic level, such as nuclear magnetic resonance (NMR) and neutron scattering[12]. Among them, the T_C of (Ba, K)(Zn, Mn)$_2As_2$ single crystal has been reported to reach 230 K[24]. (Ba, K)(Zn, Mn)$_2As_2$ was synthesized by doping Mn and K into the parent compound β-$BaZn_2As_2$ which is a direct gap (0.2 eV) semiconductor[25], where the substitution of Mn for Zn and K for Ba introduces spins and hole carriers, respectively.

In this paper, we report the successful fabrication of a new DMS material with a rather new synthesize route, which is different to the previously reported ~10 DMSs[8–19]. Instead of doping at different sites, we co-doped both Mn and Cu into the same Zn sites of $BaZn_2As_2$ to introduce local moments and carriers, respectively. A new series of DMS compounds $Ba(Zn_{1-2x}Mn_xCu_x)_2As_2$ ($0.025 \leq x \leq 0.2$) have been successfully fabricated. While the system remains semiconducting, 20% Mn and Cu doping results in a ferromagnetic transition below $T_C \sim 70$ K, followed by a magnetic glassy transition below $T_f \sim 35$ K. AC susceptibility measurements on an $x = 0.125$ sample indicate that T_f strongly depends on the applied frequencies and magnetic fields, which confirms the spin glass nature at T_f. In addition, as large as ~−53% negative magnetoresistance (MR) at a magnetic field $H = 50$ KOe has been achieved in $Ba(Zn_{0.75}Mn_{0.125}Cu_{0.125})_2As_2$, which is attributed to the suppression of spin fluctuations by magnetic field. Future work is needed to gain deeper understanding of the magnetic behavior of this system and achieve higher T_C values.

Results and Discussion

Synthesis and structural characterization. The polycrystalline specimens of $Ba(Zn_{1-2x}Mn_xCu_x)_2As_2$ ($x = 0.025, 0.075, 0.125, 0.200$) were synthesized by the solid state reaction method. Details of the synthesis and facilities used for characterization are described in the Methods section. In Fig. 1, we show the X-ray diffraction patterns for polycrystalline $Ba(Zn_{1-2x}Mn_xCu_x)_2As_2$ ($0.025 \leq x \leq 0.200$). The Rietveld refinement for $Ba(Zn_{0.85}Mn_{0.075}Cu_{0.075})_2As_2$ with parameters $R_{WP} = 10.52$ %, $R_P = 7.58$ %, $\chi^2 = 1.348$ shows that the Bragg peaks can be well indexed into the tetragonal structure with space group $I4/mmm$. The lattice parameter a increases and c decreases monotonically with the doping concentration x, indicating the successful doping of Mn and Cu into the lattice. We show the crystal structure in Fig. 1(c), which is isostructural to the parent compound of 122-type Fe-based superconductor $Ba(Fe_{1-x}Co_x)_2As_2$[26] with $T_c = 22$ K and antiferromagnet $BaMn_2As_2$ with Néel temperature $T_N = 625$ K[27]. This feature provides the possibility to make junctions with these systems though As layer. No peaks of impurities are detected for the doping levels of $x = 0.025$ and $x = 0.075$. α-$BaZn_2As_2$ with space group of $Pnma$ appears for $x = 0.125$ and becomes markable for $x = 0.20$, as marked by * in Fig. 1(a). Small traces of non-magnetic Ba_3As_{14}

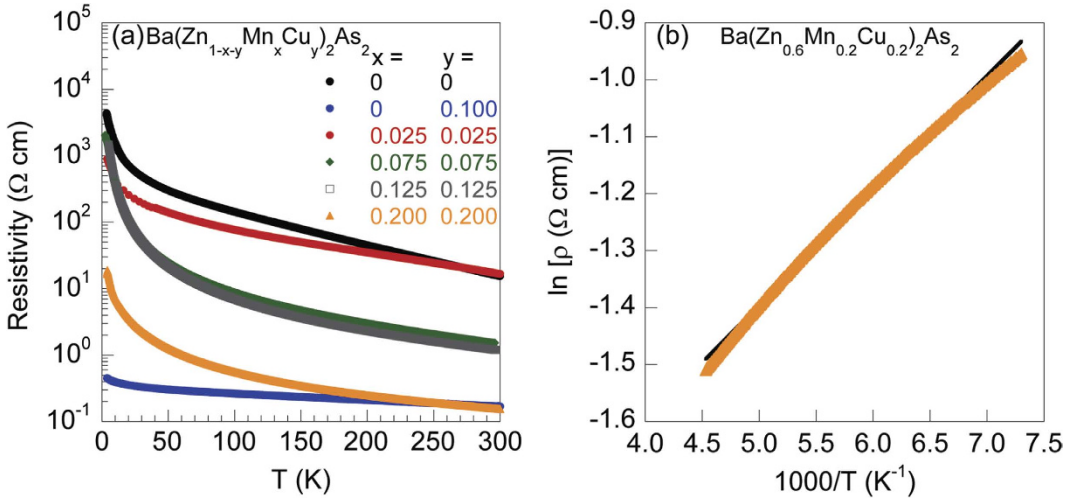

Figure 2. Electrical properties of $Ba(Zn_{1-2x}Mn_xCu_x)_2As_2$. (**a**) The temperature dependence of electrical resistivity for $BaZn_2As_2$, $Ba(Zn_{0.9}Cu_{0.1})_2As_2$ and $Ba(Zn_{1-2x}Mn_xCu_x)_2As_2$ ($x = 0.025$, 0.075, 0.125, 0.20) in logarithmic scale; (**b**) The fit of resistivity for $Ba(Zn_{0.6}Mn_{0.2}Cu_{0.2})_2As_2$ according to $\rho \propto exp(E_g/2k_BT)$.

impurity are marked as #. Both α-$BaZn_2As_2$ and Ba_3As_{14} are Pauli paramagnetic, which will not affect the magnetic behavior of $Ba(Zn_{1-2x}Mn_xCu_x)_2As_2$ discussed in the following.

Resistivity. In Fig. 2, we show the temperature dependent resistivity of the parent compound $BaZn_2As_2$, $Ba(Zn_{0.9}Cu_{0.1})_2As_2$ and $Ba(Zn_{1-2x}Mn_xCu_x)_2As_2$ ($x = 0.025$, 0.075, 0.125, 0.20). The resistivity of the parent semiconductor $BaZn_2As_2$ displays a typical semiconducting behavior. With 10% Cu doping, the resistivity of $Ba(Zn_{0.9}Cu_{0.1})_2As_2$ is heavily suppressed by an order of 4, indicating that carriers are doped. The semiconducting behavior for Mn and Cu codoped case has been conserved for x up to 20%, i.e., resistivity continuously increases with temperature decreasing from room temperature down to 4 K. The absolute value of resistivity at 4 K, however, drops from $10^3\,\Omega$ cm for $x = 0.025$ to $10\,\Omega$ cm for $x = 0.20$. We roughly fit the resistivity of $Ba(Zn_{1-2x}Mn_xCu_x)_2As_2$ ($x = 0.025$, 0.075, 0.125, 0.20) near room temperature in terms of a thermal activation function[13]. Similar approach has also been employed to (La, Sr)(Zn, Mn)AsO[13]. The fitting result for $Ba(Zn_{0.6}Mn_{0.2}Cu_{0.2})_2As_2$ is shown in Fig. 2(b) as an example. The values of energy gap E_g are between 0.031 and 0.048 eV, which are about an order of magnitude smaller than that of the parent compound $BaZn_2As_2$[25]. We have conducted Hall effect measurement on $Ba(Zn_{0.75}Mn_{0.125}Cu_{0.125})_2As_2$, but the large resistivity prevents us to accurately determine the carrier density. A preliminary result shows that the carriers are p-type with the concentration in the order of $p \sim 10^{19}\,cm^{-3}$. And the corresponding mobility is estimated to be in the order of $10^{-1}\,cm^2V^{-1}s^{-1}$. This value of carrier density is not unusual in bulk form DMSs, which is comparable to that of $(Ba_{0.9}K_{0.1})(Cd_{2-x}Mn_x)As_2$[16] and two orders of magnitude larger than that of Li(Zn, Mn)P[11], but an order of magnitude smaller than that of (Ba, K)$(Zn, Mn)_2As_2$[9] and Li(Zn, Mn)As[10].

Magnetization and hysteresis. In Fig. 3(a,b), we show the temperature dependence of magnetization for $Ba(Zn_{0.9}Mn_{0.1})_2As_2$ and $Ba(Zn_{0.9}Cu_{0.1})_2As_2$, respectively. No anomaly or transition is observed in the measured temperature range, and the moment at 2 K is only ~0.001 μ_B/(Mn or Cu atom) for both $Ba(Zn_{0.9}Mn_{0.1})_2As_2$ and $Ba(Zn_{0.9}Cu_{0.1})_2As_2$. We fit the magnetization data to a Curie-Weiss law $M = M_0 + C/(T-\theta)$ and obtained $C = 0.00456\,\mu_B$K/Mn, $\theta = -2.74$ K for $Ba(Zn_{0.9}Mn_{0.1})_2As_2$, and $C = 0.00028\,\mu_B$K/Cu, $\theta = -1.45$ K for $Ba(Zn_{0.9}Cu_{0.1})_2As_2$, indicating the paramagnetic ground state. These results indicate that doping either Mn or Cu alone into $BaZn_2As_2$ can not form any type of magnetic ordering. This feature has also been observed in LaZnAsO, where doping Mn or Fe only does not result in ferromagnetic ordering[8,12]. The magnetic character of Cu in 122-type arsenides has been investigated by density functional calculations[28] and intensive transport properties measurements[29]. Cu 3*d* bands are ~3 eV below Fermi energy (E_F), and contribute little to the density of states at E_F[28]. The 3*d* shell of Cu is completely filled with $3d^{10}$ electronic configurations[28,29]. Therefore, the valence of Cu in 122-type arsenides is +1 with nonmagnetic state S = 0[28,29]. The paramagnetic state of $Ba(Zn_{0.9}Cu_{0.1})_2As_2$ are consistent with the previous reports[28,29].

In Fig. 3(c), we show the magnetization of $Ba(Zn_{1-2x}Mn_xCu_x)_2As_2$ ($x = 0.025$, 0.075, 0.125, 0.20) with the same amount of Mn and Cu atoms doped into Zn sites of $BaZn_2As_2$. No magnetic transition has been observed for $x = 0.025$. A fit to Curie-Weiss law $M = M_0 + C/(T-\theta)$ shows that $\theta = -0.6$ K, indicating the paramagnetic ground state. For the doping level of $x = 0.075$, a strong increase of magnetization at Curie temperature $T_C = 33$ K and a bifurcation of zero field cooling (ZFC) and field cooling (FC) curves at spin freezing temperature $T_f = 12$ K are observed. T_C and T_f are enhanced with increasing doping

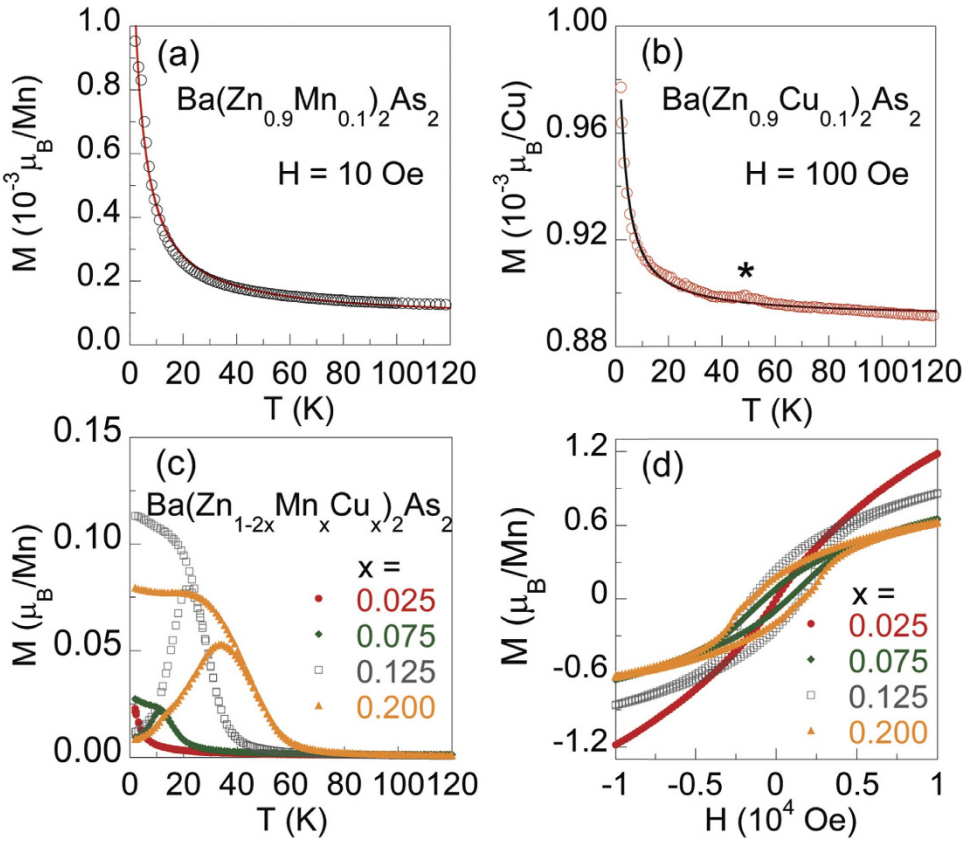

Figure 3. Magnetic properties of $Ba(Zn_{1-2x}Mn_xCu_x)_2As_2$. Temperature dependent magnetization M for (**a**) $Ba(Zn_{0.9}Mn_{0.1})_2As_2$ in an external field of $H = 10$ Oe and (**b**) $Ba(Zn_{0.9}Cu_{0.1})_2As_2$ with $H = 100$ Oe. The solid lines represent the Curie-Weiss law $M = M_0 + C/(T-\theta)$. The star marks the signal from adsorbed oxygen. (**c**) T-dependent magnetization M for $Ba(Zn_{1-2x}Mn_xCu_x)_2As_2$ ($x = 0.025$, 0.075, 0.125, 0.20) in the zero field cooling (ZFC) and field cooling (FC) modes with an external field of $H = 100$ Oe. (**d**) The isothermal magnetization measured at 2 K.

levels. With 20% doping, T_C increases to 70 K and T_f increases to 35 K. In Fig. 3(d), we present the results of isothermal magnetization measurements. For $x \geq 0.075$, clear hysteresis loops have been observed at 2 K. The coercive field becomes lager for higher x, and reaches 1600 Oe for $x = 0.20$. We should note that this value is much smaller than ~10^4 Oe of (Ba, K)(Zn, Mn)$_2$As$_2$[9]. The contrasting ground states shown in Fig. 3(a,b,c) unequivocally demonstrate that only when Zn is substituted by both Mn and Cu simultaneously, can the ferromagnetic ordering develop, which also indicates that the ferromagnetic signals result from the doping of Mn and Cu rather than impurities.

We fit the T-dependent magnetization above T_C to the Curie-Weiss formula $\chi = \chi_0 + C/(T-\theta)$ in order to obtain the Weiss temperature (θ) and effective paramagnetic moment of Mn (μ_{eff}). The best fittings show that the effective moment μ_{eff} is 4.8 ~ 5.7 μ_B/Mn for $0.025 \leq x \leq 0.20$, indicating the high spin state of Mn with the valence of +2 in the system of $Ba(Zn_{1-2x}Mn_xCu_x)_2As_2$. We tabulate the Curie temperature T_C, the spin freezing temperature T_f (the temperature where ZFC and FC curves split), the base temperature moment μ_{BT} (the values at 2 K measured from FC curves with $H = 100$ Oe), the coercive field H_c and the energy gap E_g (fitted from the resistivity data) in Table 1. T_C, T_f, θ and H_c show a trend of increasing with higher doping level x, indicating the strengthening of ferromagnetic exchange interaction with higher concentration of Mn and Cu. Meanwhile, the systematic changes of these magnetic parameters suggest that the magnetic signals in this system are not caused by impurities. On the other hand, we notice that μ_{BT} first increases from 0.027 μ_B/Mn for $x = 0.075$ to 0.110 μ_B/Mn for $x = 0.125$, but decreases to 0.079 μ_B/Mn for $x = 0.20$. This may be due to the competition of ferromagnetic and antiferromagnetic exchange interactions between Mn atoms.

To further investigate the valence of Cu and Mn, we conducted the X-ray photoelectron spectroscopy (XPS) measurements for $Ba(ZnMn_{0.2}Cu_{0.2})_2As_2$. Ba and Zn have been observed from the peaks of binding energy. But unfortunately, after very careful comparison, we haven't detected effective peaks of Cu or Mn from the binding energy. No conclusion about the valence of Cu or Mn has been achieved from the XPS measurements. We can't obtain evidence from XPS that whether Cu contribute magnetic moments

x	T_C (K)	T_f (K)	θ (K)	μ_{BT} (μ_B/Mn)	μ_{eff} (μ_B/Mn)	H_c (Oe)	E_g (eV)
0.025	—	—	−0.6	0.023	5.1	0	0.031
0.075	33	12	12.9	0.027	4.8	730	0.039
0.125	44	22	31.7	0.110	5.7	1528	0.048
0.20	70	35	50.1	0.079	5.5	1600	0.035

Table 1. Curie temperature (T_C), spin freezing temperature (T_f), Weiss temperature (θ), base temperature moment (μ_{BT}, the values at 2 K from FC curves with $H = 100$ Oe), the effective moment (μ_{eff}), coercive field (H_c), and energy gap (E_g, fitted from resistivity) for $Ba(Zn_{1-2x}Mn_xCu_x)_2As_2$ ($0.025 \leq x \leq 0.20$).

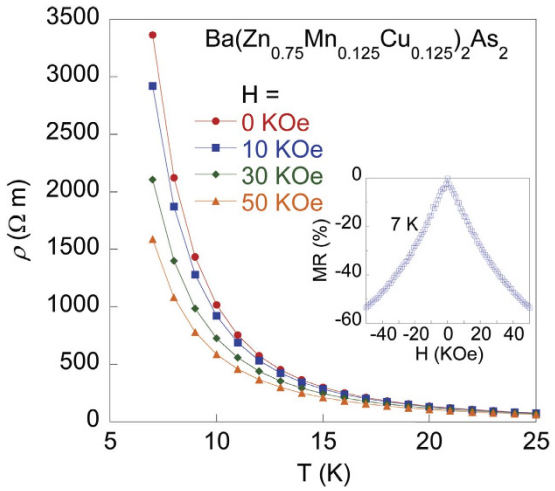

Figure 4. T-dependent magnetoresistivity for $Ba(Zn_{0.75}Mn_{0.125}Cu_{0.125})_2As_2$ under $H = 0$, 10, 30, 50 KOe. The inset shows the field dependence of magnetoresistance at 7 K from −50 KOe to 50 KOe.

or not. Magnetic resonance techniques may be used in the future to further investigate the magnetic mechanism of this system.

Magnetoresistance. We measured the magnetoresistance for $Ba(Zn_{0.75}Mn_{0.125}Cu_{0.125})_2As_2$ under the applied fields of 0, 10, 30, 50 KOe, and show the results in Fig. 4. The resistivity with different fields deviates from each other at ~22 K, and the values of ρ at 7 K monotonically drop from 3363 Ω m at 0 Oe to 1587 Ω m at 50 KOe. The magnetoresistance (defined as $[\rho(H) - \rho(0)]/\rho(0)$ at 7 K) reaches −53 % at 50 KOe. The large negative magnetoresistance has also been observed in other bulk form DMSs, such as $(Ba_{0.9}K_{0.1})(Cd_{2-x}Mn_x)_2As_2$[16] and $(Sr_{0.9}K_{0.1})(Zn_{1.8}Mn_{0.2})As_2$[17]. We tentatively attribute the negative magnetoresistance to the suppression of spin fluctuations by applied field.

AC susceptibility. We measured the AC susceptibility, χ', for the $x = 0.125$ sample at various frequencies ν under zero external field, and show the results in Fig. 5. We found that the maxima of the real part, χ', drop obviously, and T_f shifts slightly to higher temperature with the increasing AC frequencies. This feature is typically taken as signs for spin glass systems[30–37]. This kind of behavior has also been observed in $CaNi_{1-x}Mn_xGe$[30], $CeCu_4Mn$[31], $La(Fe_{1-x}Mn_x)_{1.4}Si_{1.6}$[32] and II-VI family DMS[23]. The Vogel-Fulcher law[38–41] is usually used to describe the dependence between T_f and ν,

$$\nu = \nu_0 \exp\left[-\frac{E_a}{T_f - T_0}\right], \quad (1)$$

where E_a is the activation energy, T_0 is the Vogel-Fulcher temperature, and ν_0 is the fitted frequency. We tried different values of ν_0 from 10^{10} Hz to 10^{13} Hz, which showed that the best linear fitting can be obtained when $\nu_0 \sim 10^{13}$ Hz, in good agreement with expectation for a spin-glass ($\nu_0 \sim 10^{13}$ Hz) rather than a cluster-glass ($\nu_0 \sim 10^7 - 10^9$ Hz)[42]. So ν_0 is considered as a constant value of 10^{13} Hz for this system in the following discussion. In Fig. 5(b), T_f is plotted as a function of $1/ln(\nu_0/\nu)$. The well fitted

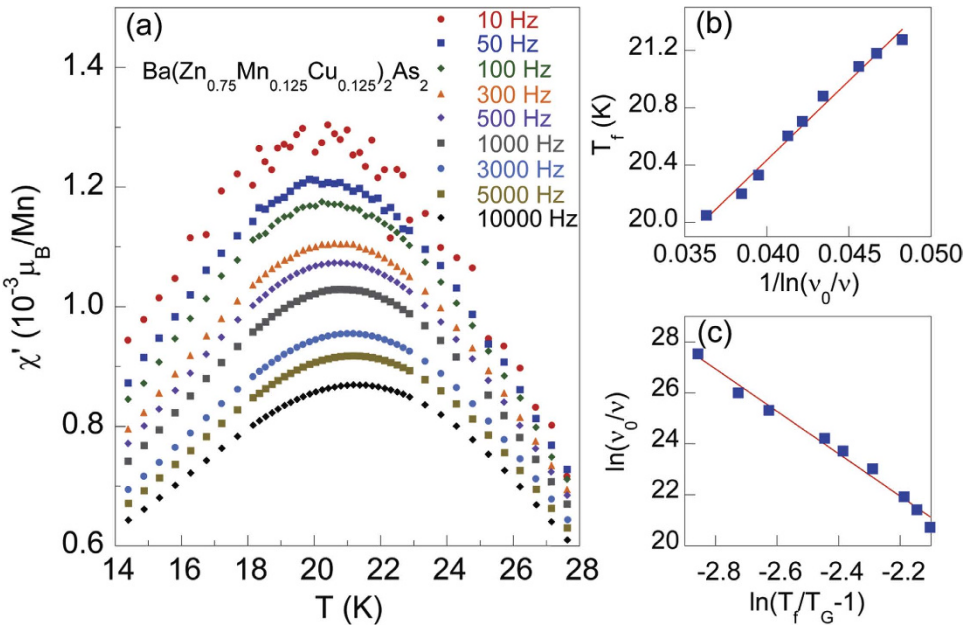

Figure 5. AC susceptibility at various frequencies for $Ba(Zn_{0.75}Mn_{0.125}Cu_{0.125})_2As_2$. (**a**) The real component χ' of AC magnetic susceptibility as a function of temperature T measured from 10 Hz to 10000 Hz. (**b**) Spin freezing temperature T_f as a function of $1/ln(\nu_0/\nu)$ fitted with the Vogel-Fulcher law. (**c**) A linear fit of $ln(\nu_0/\nu)$ versus $ln(T_f/T_0 - 1)$ with Eq. (2).

linear relation enables us to estimate the value of T_0 and E_a. T_0 is ~16 K and E_a is ~110.48 K, corresponding to E_a ~ 0.00952 eV because of $E = k_B T$ with k_B ~ 8.617×10^{-5} eV/K. So $E_g = 2E_a = 0.02$ eV, which is in the same order of magnitude as the value estimated from the fit of resistivity. The ratio $K = \Delta T_f / \left(T_f \Delta ln\nu\right)$ is usually used to distinguish the frequency sensitivity of T_f in a spin glass[40,43]. K is the order of 0.01 for spin glass systems, while $K > 0.1$ for superparamagnets[36]. For the $x = 0.125$ sample, K is estimated to be ~0.008 ± 0.002, in good agreement with the typical values reported for spin glasses[30,31,37,40].

The dynamical slowing down of spin fluctuations can also be expressed by the standard power dependence,

$$\tau = \tau_0 \left(\frac{T_f}{T_G} - 1 \right)^{-\eta}, \tag{2}$$

where $\tau = 1/\nu$ is the relaxation time, $\tau_0 = 1/\nu_0$ is set as 10^{-13} s, T_G is the spin freezing temperature, η is the dynamic exponent. When T_f approaches T_G which is the zero frequency limit, the order of τ gets much larger than τ_0, indicating that spin fluctuations significantly slow down. A linear fit of $ln(\nu_0/\nu)$ versus $ln(T_f/T_G - 1)$ according to Eq. (2) is shown in Fig. 5(c), yielding T_G ~ 18.96 K and η ~ 8.3. The value of η falls into the range of 4–12 for spin glasses[31–33,36,40,44,45], which is not cluster-glass like character[46]. η ~ 8.3 is close to 7.9, the calculated value for the three-dimensional Ising spin-glass[47,48].

In Fig. 6(a), we show the measurements of T-dependent AC susceptibility at a fixed frequency of 500 Hz with various DC fields for $Ba(Zn_{0.75}Mn_{0.125}Cu_{0.125})_2As_2$. The AC susceptibility is strongly affected by the external DC fields, i.e., the cusps smear out, the peak value of χ' decreases remarkably, and T_f shifts to lower temperature with increasing DC fields. These are all characteristic features of spin glasses[30,32,49]. The DC field dependence of the spin freezing temperature T_f can be described by the equation,

$$T_f(H) \propto 1 - bH^{\delta}. \tag{3}$$

A best fit of T_f versus H to Eq. (3) yields δ ~ 0.55. We show the plot of T_f versus $H^{0.55}$ in Fig. 6(b). δ is ~2/3 for Ising spin glass systems, and $\delta = 2$ for Heisenberg systems[50,51]. In the current case, δ is close to 2/3, indicating that the glassy state for $Ba(Zn_{1-2x}Mn_xCu_x)_2As_2$ may be explained by mean-field theory with Ising model. In Fig. 6(c), we show the imaginary component of AC susceptibility at 500 Hz with DC fields up to 3000 Oe. Similar to the case of χ', T_f decreases noticeably with increasing fields. The

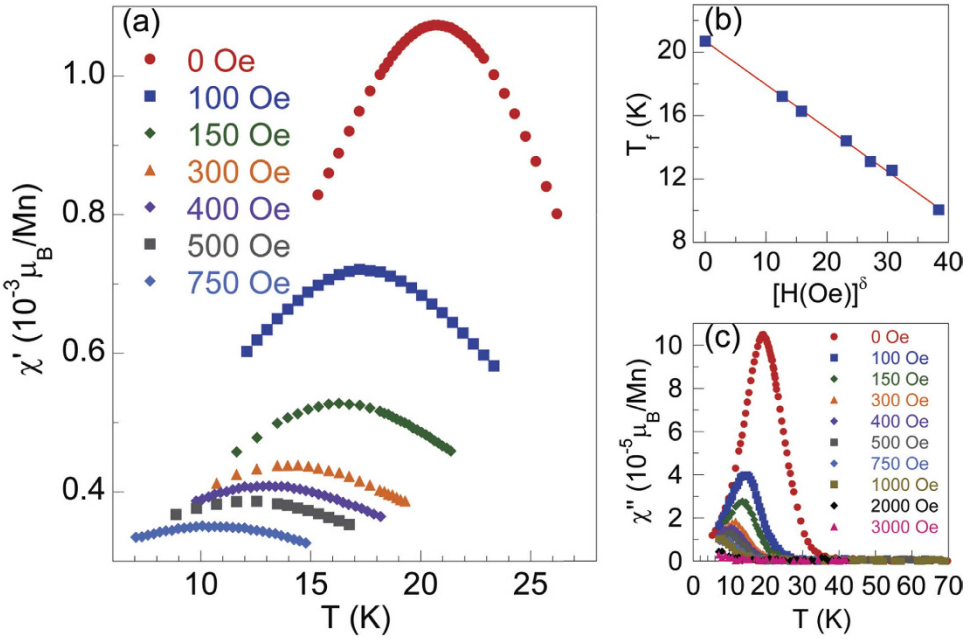

Figure 6. AC susceptibility with various DC fields for $Ba(Zn_{0.75}Mn_{0.125}Cu_{0.125})_2As_2$. (**a**) The temperature dependence of the AC susceptibility χ' measured at a frequency of 500 Hz under different applied DC fields. (**b**) T_f as a function of H^δ with $\delta = 0.55$. The straight line is a guide for eyes. (**c**) T-dependent imaginary part χ'' at 500 Hz with various DC fields from 0 to 3000 Oe.

T-dependent imaginary part χ'' of the AC susceptibility under 2000 Oe and 3000 Oe becomes almost undependent of T.

Conclusion

A bulk form diluted magnetic semiconductor $Ba(Zn_{1-2x}Mn_xCu_x)_2As_2$ ($0.025 \leq x \leq 0.2$) with maximum $T_C \sim 70$ K has been successfully synthesized. It is the first time that ferromagnetic ordering is observed when Mn and Cu are codoped into the Zn sites, where Mn substitution for Zn introduces spin and Cu substitution for Zn introduces carriers, respectively. The new system displays large negative magnetoresistance while conserving the semiconducting behavior with the doping level up to 20%. The AC susceptibility measurements show that the spin freezing temperature T_f is dependent on frequency and external field, confirming the glassy nature below 35 K. Finally, the new DMS system has a tetragonal crystal structure identical to that of "122" family of Fe-based superconductors and the antiferromagnetic system $BaMn_2As_2$, which makes it possible to make various junctions of these systems through As layer. More theoretical and experimental work are expected to further understand the properties and physics of this system.

Methods

The polycrystalline specimens of $Ba(Zn_{1-2x}Mn_xCu_x)_2As_2$ ($x = 0.025, 0.075, 0.125, 0.200$) were synthesized by the solid state reaction method. High purity elements of Zn (99.9%), Mn (99.99%), Cu (99.9%) and As (99%) were mixed, ground and pressed into pellets. The pellets were sealed in evacuated silica tubes and sintered at 800 °C for 10 hours to make the precursors $(Zn_{1-2x}Mn_xCu_x)As$. The mixture of Ba (99.2%) and $(Zn_{1-2x}Mn_xCu_x)As$ were then slowly heated to 900 °C and held for 10 hours, then 1150 °C for 15 hours before cooling down to room temperature with the furnace turned off. The handling of materials were performed in a high-purity argon filled glove box (the percentage of O_2 and $H_2O \leq 0.1$ ppm) to protect it from exposure to air. Powder x-ray diffraction was performed at room temperature using a PANalytical x-ray diffractometer (Model EMPYREAN) with monochromatic $CuK_{\alpha 1}$ radiation. The electrical resistance was measured on sintered pellets with the typical four-probe method. The DC magnetization measurements were conducted on a Quantum Design Magnetic Property Measurement System (MPMS-5). The AC susceptibility and magnetoresistance were measured on a Quantum Design Physical Property Measurement System (PPMS-9).

References

1. Munekata, H. *et al.* Diluted magnetic III-V semiconductors. *Phys. Rev. Lett.* **63,** 1849–1852 (1989).
2. Ohno, H. *et al.* (Ga, Mn)As: a new diluted magnetic semiconductor based on GaAs. *Appl. Phys. Lett.* **69,** 363–365 (1996).
3. Dietl, T. & Ohno, H. Dilute ferromagnetic semiconductors: physics and spintronic structures. *Rev. Mod. Phys.* **86,** 187–251 (2014).

4. Zutic, I., Fabian, J. & Sarma, S. Das Spintronics: fundamentals and applications. *Rev. Mod. Phys.* **76,** 323–410 (2004).
5. Jungwirth, T., Sinova, J., Masek, J., Kucera, J. & MacDonald, A. H. Theory of ferromagnetic (III, Mn)V semiconductors. *Rev. Mod. Phys.* **78,** 809–864 (2006).
6. Dietl, T., Ohno, H., Matsukura, F., Cibert, J. & Ferrand, D. Zener model description of ferromagnetism in zinc-blende magnetic semiconductors. *Science* **287,** 1019–1022 (2000).
7. Chen, L. *et al.* Enhancing the Curie temperature of ferromagnetic semiconductor (Ga, Mn)As to 200 K via nanostructure engineering. *Nano Lett.* **11,** 2584–2589 (2011).
8. Lu, J. C. *et al.* The synthesis and characterization of 1111-type diluted magnetic semiconductors $(La_{1-x}Sr_x)(Zn_{1-x}TM_x)AsO$ (TM = Mn, Fe, Co). *Europhys. Lett.* **103,** 67011 (2013).
9. Zhao, K. *et al.* New diluted ferromagnetic semiconductor with Curie temperature up to 180 K and isostructural to the "122" iron-based superconductors. *Nat. Commun.* **4,** 1442 (2013).
10. Deng, Z. *et al.* Li(Zn, Mn)As as a new generation ferromagnet based on a I-II-V semiconductor. *Nat. Commun.* **2,** 422 (2011).
11. Deng, Z. *et al.* Diluted ferromagnetic semiconductor Li(Zn, Mn)P with decoupled charge and spin doping. *Phys. Rev. B* **88,** 081203(R) (2013).
12. Ding, C. *et al.* $(La_{1-x}Ba_x)(Zn_{1-x}Mn_x)AsO$: a two-dimensional 1111-type diluted magnetic semiconductor in bulk form. *Phys. Rev. B* **88,** 041102(R) (2013).
13. Ding, C. *et al.* The suppression of Curie temperature by Sr doping in diluted ferromagnetic semiconductor $(La_{1-x}Sr_x)(Zn_{1-y}Mn_y)$ AsO. *Europhys. Lett.* **107,** 17004 (2014).
14. Yang, X. J. *et al.* Sr and Mn co-doped LaCuSO: a wide band gap oxide diluted magnetic semiconductor with T_C around 200 K. *Appl. Phys. Lett.* **103,** 022410 (2013).
15. Han, W. *et al.* Diluted ferromagnetic semiconductor (LaCa)(ZnMn)SbO isostructural to "1111" type iron pnictide superconductors. *Sci. China-Phys. Mech. Astron.* **56,** 2026–2030 (2013).
16. Yang, X. J. *et al.* K and Mn co-doped $BaCd_2As_2$: a hexagonal structured bulk diluted magnetic semiconductor with large magnetoresistance. *J. Appl. Phys.* **114,** 223905 (2013).
17. Yang, X. J. *et al.* $Sr_{0.9}K_{0.1}Zn_{1.8}Mn_{0.2}As_2$: a ferromagnetic semiconductor with colossal magnetoresistance. *Europhys. Lett.* **107,** 67007 (2014).
18. Chen, B. J. *et al.* $(Sr, Na)(Zn, Mn)_2As_2$: a diluted ferromagnetic semiconductor with the hexagonal $CaAl_2Si_2$ type structure. *Phys. Rev. B* **90,** 155202 (2014).
19. Man, H. Y. *et al.* $(Sr_3La_2O_5)(Zn_{1-x}Mn_x)_2As_2$: a bulk form diluted magnetic semiconductor isostructural to the "32522" Fe-based superconductors. *Europhys. Lett.* **105,** 67004 (2014).
20. Ding, C., Qin, C., Man, H. Y., Imai, T. & Ning, F. L. NMR investigation of the diluted magnetic semiconductor $Li(Zn_{1-x}Mn_x)P$ (x = 0.1). *Phys. Rev. B* **88,** 041108(R) (2013).
21. Ning, F. L. *et al.* Suppression of T_C by overdoped Li in the diluted ferromagnetic semiconductor $Li_{1+y}(Zn_{1-x}Mn_x)P$: a μSR investigation. *Phys. Rev. B* **90,** 085123 (2014).
22. Dunsiger, S. R. *et al.* Spatially homogeneous ferromagnetism of (Ga, Mn)As. *Nat. Mater.* **9,** 299–303 (2010).
23. Furdyna, J. K. Diluted magnetic semiconductors. *J. Appl. Phys.* **64,** R29–R64 (1988).
24. Zhao, K. *et al.* Ferromagnetism at 230 K in $(Ba_{0.7}K_{0.3})(Zn_{0.85}Mn_{0.15})_2As_2$ diluted magnetic semiconductor. *Chin. Sci. Bull.* **59,** 2524–2527 (2014).
25. Xiao, Z. W. *et al.* Epitaxial growth and electronic structure of a layered zinc pnictide semiconductor, β-$BaZn_2As_2$. *Thin Solid Films* **559,** 100–104 (2014).
26. Sefat, A. S. *et al.* Superconductivity at 22 K in Co-doped $BaFe_2As_2$ crystals. *Phys. Rev. Lett.* **101,** 117004 (2008).
27. Singh, Y. *et al.* Magnetic order in $BaMn_2As_2$ from neutron diffraction measurements. *Phys. Rev. B* **80,** 100403(R) (2009).
28. Singh, D. J. Electronic structure of $BaCu_2As_2$ and $SrCu_2As_2$: *sp*-band metals. *Phys. Rev. B* **79,** 153102 (2009).
29. Anand, V. K. *et al.* Crystal growth and physical properties of $SrCu_2As_2$, $SrCu_2Sb_2$, and $BaCu_2Sb_2$. *Phys. Rev. B* **85,** 214523 (2012).
30. Liu, X. F., Matsuishi, S., Fujitsu, S. & Hosono, H. Spin-glass-like behavior of $CaNi_{1-x}Mn_xGe$. *Phys. Rev. B* **84,** 214439 (2011).
31. Tolińśki, T. & Synoradzki, K. Spin-glass behavior in $CeCu_xNi_{4-x}Mn$ and $Ce_{0.9}Nd_{0.1}Ni_4Mn$ compounds. *Intermetallics* **19,** 62–67 (2011).
32. Wang, F. *et al.* Spin-glass behavior in $La(Fe_{1-x}Mn_x)_{11.4}Si_{1.6}$ compounds. *Phys. Rev. B* **69,** 094424 (2004).
33. Li, D. X., Yamamura, T., Nimori, S. & Shiokawa, Y. Re-entrant spin-glass behaviour in $CeAu_2Si_2$. *J. Alloys Comp.* **451,** 461–463 (2008).
34. Li, D. X. *et al.* Evidence for the formation of the spin-glass state in U_2PdSi_3. *Phys. Rev. B* **57,** 7434–7437 (1998).
35. Hong, C. S., Kim, W. S., Chi, E. O., Hur, N. H. & Choi, Y. N. Role of rare earth ion in spin glass behavior for $R_{0.7}Sr_{1.3}MnO_4$. *Chem. Mater.* **14,** 1832–1838 (2002).
36. Greedan, J. E. *et al.* Frustrated pyrochlore oxides, $Y_2Mn_2O_7$, $Ho_2Mn_2O_7$, and $Yb_2Mn_2O_7$: bulk magnetism and magnetic microstructure. *Phys. Rev. B* **54,** 7189–7200 (1996).
37. Soldevilla, J. G., Gómez Sal, J. C., Blanco, J. A., Espeso, J. I. & Feránndez, J. R. Phase diagram of the $CeNi_{1-x}Cu_x$ Kondo system with spin-glass-like behavior favored by hybridization. *Phys. Rev. B* **61,** 6821–6825 (2000).
38. Vogel, H. The law of the relationship between viscosity of liquids and the temperature. *Phys. Z* **22,** 645–646 (1921).
39. Fulcher, G. S. Analysis of recent measurements of the viscosity of glasses. *J. Am. Ceram. Soc.* **8,** 339–355 (1925).
40. Mydosh, J. A. *Spin Glasses: An Experimental Introduction* (Taylor & Francis, London, 1993).
41. Tholence, J. L. On the frequency dependence of the transition temperature in spin glasses. *Solid State Commun.* **35,** 113–117 (1980).
42. Phan, M. H. *et al.* Magnetism and cluster glass dynamics in geometrically frustrated $LuFe_2O_4$. *J. Appl. Phys.* **105,** 07E308 (2009).
43. Mulder, C. A. M., Duyneveldt, A. J. van & Mydosh, J. A. Susceptibility of the CuMn spin-glass: frequency and field dependences. *Phys. Rev. B* **23,** 1384–1396 (1981).
44. Gunnarsson, K. *et al.* Dynamics of an Ising spin-glass in the vicinity of the spin-glass temperature. *Phys. Rev. Lett.* **61,** 754–757 (1988).
45. Jonason, K., Mattsson, J. & Nordblad, P. Dynamic susceptibility of a reentrant ferromagnet. *Phys. Rev. B* **53,** 6507–6513 (1996).
46. Vijayanandhini, K., Simon, Ch., Pralong, V., Caignaert, V. & Raveau, B. Spin glass to cluster glass transition in geometrically frustrated $CaBaFe_{4-x}Li_xO_7$ ferrimagnets. *Phys. Rev. B* **79,** 224407 (2009).
47. Ogielski, A. T. Dynamics of three-dimensional Ising spin glasses in thermal equilibrium. *Phys. Rev. B* **32,** 7384–7398 (1985).
48. Gubkin, A. F., Sherstobitova, E. A., Terentyev, P. B., Hoser, A. & Baranov, N. V. A cluster-glass magnetic state in R_5Pd_2 (R = Ho, Tb) compounds evidenced by AC-susceptibility and neutron scattering measurements. *J. Phys.: Condens. Matter* **25,** 236003 (2013).
49. Zhou, G. F. & Bakker, H. Spin-glass behavior of mechanically milled crystalline $GdAl_2$. *Phys. Rev. Lett.* **73,** 344–347 (1994).
50. Almeida, J. R. L. De & Thouless, D. J. Stability of the Sherrington-Kirkpatrick solution of a spin glass model. *J. Phys. A: Math. Gen.* **11,** 983–990 (1978).
51. Lefloch, F., Hammann, J., Ocio, M. & Vincent, E. Spin glasses in a magnetic field: phase diagram and dynamics. *Physica B: Condens. Matter* **203,** 63–74 (1994).

Acknowledgements

The work at Zhejiang was supported by National Basic Research Program of China (No. 2014CB921203, 2011CBA00103), NSF of China (No. 11274268, No. 11574265), Zhejiang Provincial Natural Science Foundation of China (LR15A040001). F.L. Ning acknowledges helpful discussions with S. Maekawa and D. C. Johnston.

Author Contributions

H.M., S.G., Y.S., Y.G., B.C., H.W. and C.D. performed the experiments. H.M., S.G., C.D. and F.N. analyzed the results. H.M. and F.N. prepared the figures and wrote the paper. F.N. designed and directed the research. All authors reviewed the manuscript.

Additional Information

Competing financial interests: The authors declare no competing financial interests.

How to cite this article: Man, H. Y. *et al.* $Ba(Zn_{1-2x}Mn_xCu_x)_2As_2$: A Bulk Form Diluted Ferromagnetic Semiconductor with Mn and Cu Codoping at Zn Sites. *Sci. Rep.* **5**, 15507; doi: 10.1038/srep15507 (2015).